



## Article

# Numerical Research on Biomass Gasification in a Quadruple Fluidized Bed Gasifier

Linbo Yan <sup>1,\*</sup>, Ziyue Jia <sup>1</sup>, Ziliang Wang <sup>2</sup>, Boshu He <sup>1</sup>  and Baizeng Fang <sup>3,\*</sup> 

<sup>1</sup> Institute of Combustion and Thermal System, School of Mechanical, Electronic and Control Engineering, Beijing Jiaotong University, Beijing 100044, China

<sup>2</sup> School of Energy and Power Engineering, Shandong University, Jinan 250061, China

<sup>3</sup> Department of Chemical and Biological Engineering, University of British Columbia, 2360 East Mall, Vancouver, BC V6T 1Z3, Canada

\* Correspondence: lbyan@bjtu.edu.cn (L.Y.); baizengfang@163.com (B.F.)

**Abstract:** Utilization of bioenergy with carbon capture can realize carbon-negative syngas production. The quadruple fluidized bed gasifier (QFBG) integrates a chemical looping oxygen generation process and a dual fluidized bed gasifier with limestone as bed material. It is one promising device that can convert biomass to H<sub>2</sub>-rich syngas whilst capturing CO<sub>2</sub> with little energy penalty. However, experimental or numerical simulation of QFBG is rarely reported on due to its complex structure, hindering the further commercialization and deployment of QFBG. In this work, a new computational fluid dynamics (CFD) solver is proposed to predict the complex physicochemical processes in QFBG based on the multi-phase particle in cell (MPPIC) methodology with the assistance of the open source software, OpenFOAM. The solver is first validated against experimental data in terms of hydrodynamics and reaction kinetics. Then, the solver is used to investigate the QFBG property. It is found that the QFBG can operate stably. The cold gas efficiency, H<sub>2</sub> molar fraction, and CO<sub>2</sub> capture rate of the QFBG are predicted to be 87.2%, 93.3%, and 90.5%, respectively, which is promising. It is believed that the solver can give reliable predictions for similar fluidized bed reactors.

**Keywords:** biomass-steam gasification; quadruple fluidized bed gasifier (QFBG); carbon capture; chemical looping air separation; multi-phase particle in cell



**Citation:** Yan, L.; Jia, Z.; Wang, Z.; He, B.; Fang, B. Numerical Research on Biomass Gasification in a Quadruple Fluidized Bed Gasifier. *Processes* **2022**, *10*, 2526. <https://doi.org/10.3390/pr10122526>

Academic Editors: Antonio Galgano and Carmen Branca

Received: 30 October 2022

Accepted: 23 November 2022

Published: 28 November 2022

**Publisher's Note:** MDPI stays neutral with regard to jurisdictional claims in published maps and institutional affiliations.



**Copyright:** © 2022 by the authors. Licensee MDPI, Basel, Switzerland. This article is an open access article distributed under the terms and conditions of the Creative Commons Attribution (CC BY) license (<https://creativecommons.org/licenses/by/4.0/>).

## 1. Introduction

The whole world is fighting against global warming so as to keep the atmosphere's CO<sub>2</sub> concentration well below the critical value of 450 ppm [1]. To meet the requirement of the Paris Agreement [2], it has been reported that carbon-negative power generation technologies should be developed and deployed [3]. Bioenergy with carbon capture provides such a transformative route, not only because biomass is carbon-neutral during the thermal conversion process, but also because biomass is the fourth largest fuel source following coal, oil, and gas on the earth [4]. However, low calorific value is one essential drawback that hinders the direct utilization of biomass [5]. Converting biomass into high-quality syngas via gasification can well solve this issue. The syngas from biomass can then be used for power generation or for utilization in the steel industry [6,7]. Because biomass is hard to grind into fine powder but relatively easy to compress into pellets, a fluidized bed is then the proper reactor for biomass gasification. A dual fluidized bed gasifier (DFBG), which consists of a bubbling fluidized bed gasifier and a fast fluidized bed combustor, can generate high-quality syngas by avoiding direct contact between air and syngas [8]. However, DFBG cannot capture CO<sub>2</sub> in situ, so carbon-negative gasification cannot be realized. Based on DFBG, a quadruple fluidized bed gasifier (QFBG) is conceptually designed by integrating the chemical looping oxygen generation technology and DFBG [9]. The chemical looping oxygen generation process is also realized in a dual fluidized bed with Mn<sub>2</sub>O<sub>3</sub> and Mn<sub>3</sub>O<sub>4</sub> as bed material. Thereby, there are four fluidized bed reactors

including a bubbling fluidized bed gasifier for biomass gasification and CaO carbonation, a fast fluidized bed oxyfuel combustor for residual char combustion and CaCO<sub>3</sub> calcination, a bubbling fluidized bed oxidation reactor for Mn<sub>3</sub>O<sub>4</sub> oxidation, and a fast fluidized bed reduction for Mn<sub>2</sub>O<sub>3</sub> reduction. With the four integrated fluidized bed reactors, biomass can be converted into H<sub>2</sub>-rich syngas. Since the bed materials are circulated inside the reactors, the heat absorbed and the heat released can be theoretically balanced. However, due to the formidable complexity of QFBG, related experiments or numerical simulations are seldom reported.

Liu [10] did the thermodynamic modeling of biomass sorption-enhanced chemical looping gasification, and the energy efficiency of this technology was found to be 64.6%. Pröll [11] studied the H<sub>2</sub>-rich syngas production by selective CO<sub>2</sub> removal during biomass gasification in a 100 kW DFGB using the thermodynamic equilibrium approach and found that H<sub>2</sub> volume fraction in the dry syngas could reach 65–75%, and CO<sub>2</sub> volume fraction was in the range of 6–13%. Koppatz [12] experimentally studied the calcium-enhanced biomass gasification process in an 8-MW DFGB and found that the H<sub>2</sub> volume fraction in the syngas was about 50%, and the CO<sub>2</sub> volume fraction was about 12.3%. The low H<sub>2</sub> fraction was probably caused by the low temperature (about 650 °C), and high steam partial pressure. Hejazi [13] once modeled biomass steam gasification in a DFGB with lime-based CO<sub>2</sub> capture using the stoichiometric equilibrium method. It was found that the CO<sub>2</sub> capture rate could be over 70%. Cormos [14] studied the chemical looping air separation cycle for decarbonized power generation based on oxyfuel combustion in terms of energy and cost. It was found that the manganese looping cycle could be more efficient than the cryogenic process, and could improve the net efficiency by 2–3.5 percentage points. The CO<sub>2</sub> capture penalty was reduced to 5–7 net energy efficiency points. Mei [15] studied the reactivity and lifetime of an oxygen releasable manganese ore and found that repeatable O<sub>2</sub> gas release was available, and the reactivity and lifetime of Mn ore were better than the often-used ilmenite. Yan [9] studied the biomass/coal co-gasification properties in a DFGB reactor using a one-dimensional model with the assistance of the commercial software, Aspen Plus. The cold gas efficiency was up to 78.9% under the proposed optimum condition. This model coupled the fluidized bed hydrodynamics and reaction kinetics. However, the model is one-dimensional and the research object is DFGB. Yan [16] studied the property of QFBG using the commercial software, Aspen Plus. It was found that the H<sub>2</sub> mole fraction in the dry syngas is higher than 70%, the CO<sub>2</sub> mole fraction in the dry flue gas is around 97%, and the net carbon discharge can be negative when the biomass blending ratio is over 0.5. The QFBG property was preliminarily studied. However the research simplified QFBG as one-dimensional, so the predictions cannot reflect the practical situation. Yan [17] studied the biomass steam gasification process in a DFGB reactor based on the granular kinetic theory (GKT) with the assistance of the commercial software, Fluent. The H<sub>2</sub> mole fraction was predicted to be 46.62%, and the cold gas efficiency was 82.9%. Although this is a three-dimensional simulation, the object is DFGB, which is quite simple compared with QFBG. Moreover, GKT treated the bed material and solid fuel as a fluid phase, which requires that the particle dimension should be uniform rather than dispersed. Yan [18] also studied the property of the DFGB reactor based on the multiphase particle in cell (MPPIC) method with the assistance of the open-source software, OpenFOAM. The model predictions were compared with experimental data, and the operating characteristics of the DFGB were predicted. The MPPIC method considered all particles as computation parcels and track each parcel in Lagrangian coordinates, so it is more advanced than GKT for fluidized bed simulation. However, the research object was still DFGB rather than QFBG. Pissot [19] compared four DFGB configurations including heat supply by air combustion, oxyfuel combustion, chemical looping gasification, and electrical thermal, and found that the oxyfuel and the chemical looping gasification scheme exhibited the lowest energy demand for CO<sub>2</sub> separation. This is also the reason why QFBG integrates chemical looping technology. Wang [20] predicted hydrogen production via chemical looping reforming in a DFGB reactor based on the granular kinetic theory. A bubble-structure-dependent

drag coefficient model was proposed and the model predictions were validated against experimental data.

From a literature review, it can be concluded that calcium-enhanced biomass gasification can increase the  $H_2$  fraction and decrease the  $CO_2$  fraction in dry syngas. However, the stripped carbon cannot be captured if air is used as an oxidizer for the calcination process. To gasify biomass whilst capturing  $CO_2$ , oxyfuel combustion should be introduced. According to literature reports, the more efficient manganese-based chemical looping air separation approach is chosen and is coupled with the calcium-based DFBC to form the QFBG in this work. Although the QFBG property has been studied with the Aspen Plus platform, the three-dimensional simulation of QFBG has not been carried out. This work aims to further study the physicochemical processes of QFBG with the computational fluid dynamics approach so that the QFBG characteristics can be known better. The processes in QFBG include the fluidization of different particles like limestone, manganese ore, and biomass, heterogeneous reactions like biomass pyrolysis and char gasification, homogeneous reactions, and the coupling of hydrodynamics with chemical reactions. There is currently no solver that can simulate such a complex process, so a new solver based on OpenFOAM is proposed and validated in this work.

## 2. Materials and Methods

As shown in Figure 1, the QFBG reactor investigated in this work is composed of a cylinder-shaped bubbling fluidized bed gasifier (BFBG) with a height of 1.5 m and diameter of 0.16 m, a cylinder-shaped fast fluidized bed combustor (FFBC) with a height of 2.26 m and diameter of 0.06 m, a cylinder-shaped bubbling fluidized bed oxidation (BFBO) reactor with a height of 1.5 m and diameter of 0.16 m, and a cylinder-shaped fast fluidized bed reduction (FFBR) reactor with a height of 2.26 m and diameter of 0.06 m. The four fluidized beds are connected by pipes with a diameter of 0.06 m. The cyclone diameter is 0.151 m at the top and 0.06 m at the bottom. The total height of the cyclone is 0.32 m and the height of the cone section is 0.2 m. The height of the loop seal is 0.205 m. The bottoms of the bubbling fluidized bed reactors are 0.4 m higher than those of the fast fluidized bed reactors. The recirculated bed material enters the fluidized bed reactors at a height of 0.85 m from the bottom. The super-heated steam is used as the gasification agent for the gasifier. The  $O_2/CO_2$  mixture gas is used as the oxidant for the oxidation reactor. The flue gas is discharged from the reactor outlet.

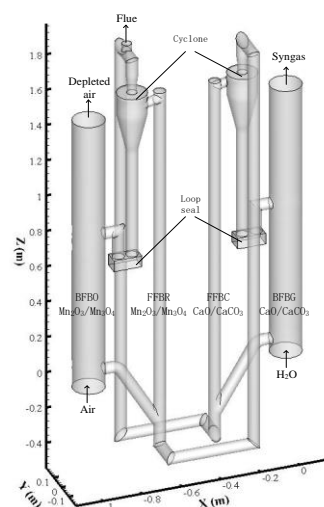


**Figure 1.** Sketch of the quadruple fluidized bed gasifier.

To simulate the physicochemical processes in QFBG, a new solver based on the MPPIC method in OpenFOAM was compiled so that it could simultaneously consider the gas-solid flow hydrodynamics and the dominant chemical reactions. The PIMPLE algorithm [21] was

chosen to solve the partial differential equation sets. The Euler scheme was chosen to implicitly discrete the transient term. The Gauss linear scheme was chosen to discrete the gradient term. The Gauss linear limited scheme was used to discrete the Laplacian term. The Gauss upwind unlimited scheme and the Gauss limited linear scheme were used to discrete the divergence terms. The linear scheme was used to interpolate values from the cell center to the face center. The limited scheme was used for the surface normal gradient terms. For the pressure correction equation, the relax factor was set to 0.5, while for other equations, the relax factors were set to 0.7. The final residuals of all these equations during iterations were controlled to be smaller than  $10^{-6}$ . For all the simulations, grid sensitivities were implemented to make sure that the simulation results were independent of the grid size.

### 2.1. The Governing Equations

To mathematically describe the physicochemical processes in the QFBG reactor, governing equations for both the gas phase and solid phase are listed in Tables 1 and 2.

**Table 1.** Governing equations for gas phase.

The continuity equations	
$\frac{\partial(\theta_g \rho_g)}{\partial t} + \nabla \cdot (\theta_g \rho_g u_g) = S_{gm}$	(1)
The momentum equations	
$\frac{\partial(\theta_g \rho_g u_g)}{\partial t} + \nabla \cdot (\theta_g \rho_g u_g u_g) = -\theta_g \nabla p + F + \theta_g \rho_g g + \nabla \cdot (\theta_g \tau_g)$	(2)
The energy equations	
$\frac{\partial(\theta_g \rho_g h_g)}{\partial t} + \nabla \cdot (\theta_g \rho_g u_g h_g) = \nabla \cdot (\lambda_g \theta_g \nabla T_g) + \theta_g \left( \frac{\partial p}{\partial t} + u_g \cdot \nabla p \right) + \phi + \dot{q}_D + \dot{Q} + S_h + S_{h,p}$	(3)
The species transportation equation	
$\frac{\partial(\theta_g \rho_g Y_{g,i})}{\partial t} + \nabla \cdot (\theta_g \rho_g u_g Y_{g,i}) = \nabla \cdot (\rho_g D \theta_g \nabla Y_{g,i}) + \delta \dot{m}_{i,chem} + \delta \dot{m}_{p,i,chem}$	(4)
The turbulence equations	
$\frac{\partial(\theta_g \rho_g \varepsilon)}{\partial t} + \nabla \cdot (\theta_g \rho_g u_g \varepsilon) = \nabla \cdot \left( \theta_g \left( \mu_g + \frac{\mu_t}{\sigma_\varepsilon} \right) \nabla \varepsilon \right) + \theta_g \frac{\varepsilon}{k} (C_{\varepsilon 1} G_k - C_{\varepsilon 2} \rho_g \varepsilon)$	(5)

**Table 2.** Governing equations for solid phase.

The particle distribution function	
$\frac{\partial f}{\partial t} + \frac{\partial(f u_s)}{\partial x} + \frac{\partial(f A)}{\partial u_s} = \frac{f_D - f}{\tau_D}$	(6)
The particle acceleration	
$A = \frac{d u_s}{d t} = D_s (u_g - u_s) - \frac{\nabla p}{\rho_s} - \frac{\nabla \tau_s}{\theta_s \rho_s} + g + F_s$	(7)
The particle normal stress	
$\tau_s = \frac{P_s \theta_s^\beta}{\max[\theta_{cp} - \theta_s, \gamma(1 - \theta_s)]} \delta$	(8)
The particle volume fraction	
$\theta_s = 1 - \theta_g = \iint f \frac{m_s}{\rho_s} d m_s d u_s$	(9)

In Table 1,  $\theta_g$ ,  $\rho_g$ ,  $u_g$ ,  $S_{gm}$ , and  $t$  denote the gas volume fraction, the gas density, the gas velocity, mass source, and the residence time, respectively;  $p$ ,  $F$ ,  $g$ , and  $\tau_g$  denote the gas thermodynamic pressure, the interphase momentum transfer rate, the gravitational acceleration and the gas stress tensor; respectively,  $h_g$ ,  $T_g$ , and  $\lambda_g$  denote the gas enthalpy, the gas temperature and the gas mixture thermal conductivity, respectively;  $\phi$ ,  $\dot{q}_D$ ,  $\dot{Q}$ ,  $S_{h,p}$ , and  $S_h$  denote the viscous dissipation, enthalpy diffusion, radiation source, homogeneous reaction enthalpy source and heterogeneous reaction enthalpy source, respectively;  $Y_{g,i}$ ,  $D$ ,  $\delta \dot{m}_{i,chem}$ ,

and  $\delta \dot{m}_{p,i,chem}$  denote the mass fraction of species  $i$ , the effective mass diffusivity, the net production rate of species  $i$  due to homogeneous reactions and the net production rate of species  $i$  due to the heterogeneous reactions, respectively;  $k$ ,  $\varepsilon$ , and  $\mu_t$  are the turbulence kinetic energy, turbulence dissipation rate and the turbulent viscosity, respectively.

In Table 2,  $A$ ,  $u_s$ ,  $f_D$ , and  $\tau_D$  denote the particle acceleration, velocity, the probability distribution function of particle velocity, and the collision damping time, respectively;  $D_s$ ,  $\theta_s$ ,  $\rho_s$ ,  $\tau_s$ , and  $F_s$  are the interphase momentum transfer coefficient calculated with Ergun, and Wen and Yu equations, the solids volume fraction, the solid density, the particle normal stress and the particle friction per unit mass;  $P_s$ ,  $\beta$ , and  $\gamma$  are constants;  $\theta_{cp}$  is the close-packed particle volume fraction; and  $\delta$  is the Kronecker delta.

## 2.2. The Reaction Kinetics

The dominant reactions in QFB include the biomass gasification reactions, the CaO/CaCO<sub>3</sub> carbonation/calcination reactions, and the Mn<sub>2</sub>O<sub>3</sub>/Mn<sub>3</sub>O<sub>4</sub> reduction/oxidation reactions. The biomass gasification reactions include moisture evaporation, dry biomass pyrolysis, and char gasification. The moisture evaporation rate is calculated according to Equation (10). The pyrolysis kinetics is calculated with Equation (11). The other homogeneous and heterogeneous reaction kinetic correlations are listed in Table 3. The CaO carbonation kinetics is calculated by Equation (12) and the CaCO<sub>3</sub> calcination kinetics is calculated with Equation (13). The Mn<sub>2</sub>O<sub>3</sub> reduction kinetics is calculated with Equation (14), and the Mn<sub>3</sub>O<sub>4</sub> oxidation kinetics is calculated with Equation (15).

$$\frac{dm_s}{dt} = \frac{Sh_{AB} D_{i,m}}{d_p} \left( \frac{p_{sat}(T_p)}{RT_p} - X_i \frac{p}{RT_\infty} \right) A_s M_w \quad (10)$$

where,  $Sh_{AB}$  is Sherwood number;  $d_p$  is the particle diameter;  $D_{i,m}$  denotes the vapor diffusion coefficient;  $p_{sat}$  is the saturation pressure at a specific particle temperature  $T_p$ ;  $X_i$  is the local bulk mole fraction of species  $i$ ;  $p$  is the local absolute pressure;  $T_\infty$  is the local bulk temperature of the gas;  $A_s$  is the particle surface area;  $M_w$  is the H<sub>2</sub>O molar weight.

$$\frac{dm_{devol}}{dt} = -5 \times 10^6 \exp\left(-\frac{1.2 \times 10^8}{RT_p}\right) m_{devol} \quad (11)$$

where,  $m_{devol}$  is the residual volatile mass;  $R$  is the ideal gas constant. Char is assumed to be carbon, and the volatile further decomposed into H<sub>2</sub>, CO, CO<sub>2</sub>, and CH<sub>4</sub> based on element mass balance.

$$r_{cab} = 5.007 \times 10^{-3} \times \exp\left(\frac{-20,300}{8.3145 \times T}\right) \times (P_{CO_2} - P_{CO_2,eq}) \times m_{CaO} \quad (12)$$

where,  $P_{CO_2,eq}$  and  $P_{CO_2}$  denote the CO<sub>2</sub> partial pressures (atm) at the equilibrium state and at any state, respectively;  $m_{CaO}$  is the mass flow rate (kg/s) of CaO.

$$r_{cal} = 252,015.2 \times \exp\left(\frac{-91,700}{8.3145 \times T}\right) \times (1 - x_{cal})^{2/3} \times (C_{CO_2,eq} - C_{CO_2}) \quad (13)$$

where,  $x_{cal}$  denotes the conversion of CaCO<sub>3</sub>;  $C_{CO_2,eq}$  and  $C_{CO_2}$  denote the CO<sub>2</sub> concentrations (kmol/m<sup>3</sup>) at the equilibrium state and at any state.

$$r_{Mn_2} = 0.936667 \times \exp\left(\frac{-544.42}{8.3145 \times T}\right) \times (1 - x_{Mn_2})^{1.2} \quad (14)$$

where,  $x_{Mn_2}$  denotes the conversion of Mn<sub>2</sub>O<sub>3</sub>.

$$r_{Mn_3} = -0.00428 + 0.005354 \times \exp\left(-2 \times ((T - 1001.686)/311.358)^2\right) \times (C_{O_2} - C_{O_2,eq})^{0.467} \quad (15)$$

where,  $C_{O_2,eq}$  and  $C_{O_2}$  denote the oxygen concentrations ( $\text{mol/m}^3$ ) at the equilibrium state and at any state.

**Table 3.** Dominant reactions and corresponding kinetic correlations.

	Reactions	Kinetic Correlations ( $\text{kmol/m}^3/\text{s}$ )	Ref.
R1	$\text{CH}_4 + \text{H}_2\text{O} = \text{CO} + \text{H}_2$	$r_1 = 0.312 \exp(-30,000/(1.987T_g))C_{\text{CH}_4}$	[22]
R2	$\text{CO} + \text{H}_2\text{O} = \text{CO}_2 + \text{H}_2$	$r_2 = 2.78 \times 10^3 \exp(-1.26 \times 10^7/R/T_g)C_{\text{CO}}C_{\text{H}_2\text{O}}$	[23]
R3	$\text{CO}_2 + \text{H}_2 = \text{CO} + \text{H}_2\text{O}$	$r_3 = 9.59 \times 10^4 \exp(-4.66 \times 10^7/R/T_g)C_{\text{CO}_2}C_{\text{H}_2}$	[23]
R4	$\text{CO} + 0.5\text{O}_2 = \text{CO}_2$	$r_4 = 1.0 \times 10^{10} \exp(-15,154.25/T_g)C_{\text{CO}}C_{\text{O}_2}^{0.5}C_{\text{H}_2\text{O}}^{0.5}$	[24]
R5	$\text{H}_2 + 0.5\text{O}_2 = \text{H}_2\text{O}$	$r_5 = 2.2 \times 10^9 \exp(-13,109.63/T_g)C_{\text{H}_2}C_{\text{O}_2}$	[24]
R6	$\text{CH}_4 + 2\text{O}_2 = \text{CO}_2 + 2\text{H}_2\text{O}$	$r_6 = 2.119 \times 10^{11} \exp(-24,379.097/T_g)C_{\text{CH}_4}^{0.2}C_{\text{O}_2}^{1.3}$	[25]

### 2.3. Model Validation

#### Solution Scheme

The new solver was built based on OpenFOAM 3.0.0 [26]. The ReactingMultiphase Cloud and the MPPIC Cloud were combined to form the User-defined ReactingMultiphase MPPIC Cloud so that the four-way interaction could be considered for the reacting parcels. The homogeneous reactions were determined in the constant package of each case. The pyrolysis reactions were determined in the DevolatilisationModel package in the src library. The heterogeneous reactions were determined in the surface ReactionModel package in the src library. Before the final simulation, many types of grids and grid numbers were tested for the simulation of the complex process. To obtain a satisfying solution convergence when solving the equation sets for dense particle flow with chemical reaction, the computational domains of the fluidized bed reactors were meshed with the stairstep scheme to generate the hexahedron cells so that perfect grid orthogonality can be reached. To balance the calculation accuracy and the calculation efficiency, the set of stairstep grids with about 18,000 cells was chosen for the QFBG simulation. The transient time step was set variable to maintain the Courant number not bigger than 0.3. The residuals of the energy equations were restricted below  $1 \times 10^{-6}$ , and those of the other equations were restricted below  $1 \times 10^{-3}$  to ensure iteration accuracy.

## 3. Results and Discussions

### 3.1. Model Validation

To ensure the rationality of the solver and solution methods, the simulation predictions were first compared with reported experiment data including the voidage distribution in a cold state traveling fluidized bed (Exp. I) [27] and the outlet species molar fractions from a hot state calcium enhanced fluidized bed gasifier (Exp. II) [28]. The operating conditions of the two experimental fluidized beds are listed in Table 4, and the comparison results are shown In Figure 2a,b. The biomass composition is given in Table 5.

**Table 4.** Experimental parameters.

Experiments	Dimension	Superficial Velocity	Bed Material	Bed Weight	Fuel Type	Fuel Flow Rate	Operating Temperature
Exp. I	R66.7 × H2320 mm	0.3 m/s	SiO <sub>2</sub>	30.4 kg	none	none	None
Exp. II	75 × 120 × 2500 mm	0.24 m/s	CaO	37.5 kg	Biomass	25 kg/h	645 °C

From Figure 2, it is seen that good agreement between the model predictions and the reported experimental data can be obtained with the solver and the corresponding solution methods. The errors between prediction and Exp. I data are mainly caused by the simplification of the physical particles into parcels that can include thousands of real

particles so as to reduce the computational cost. The errors between model predictions with Exp. II data are mainly caused by the simplification of the biomass steam gasification process into finite global reactions, and the kinetic parameters are general ones and are not specifically generated for the gasification process in this work.

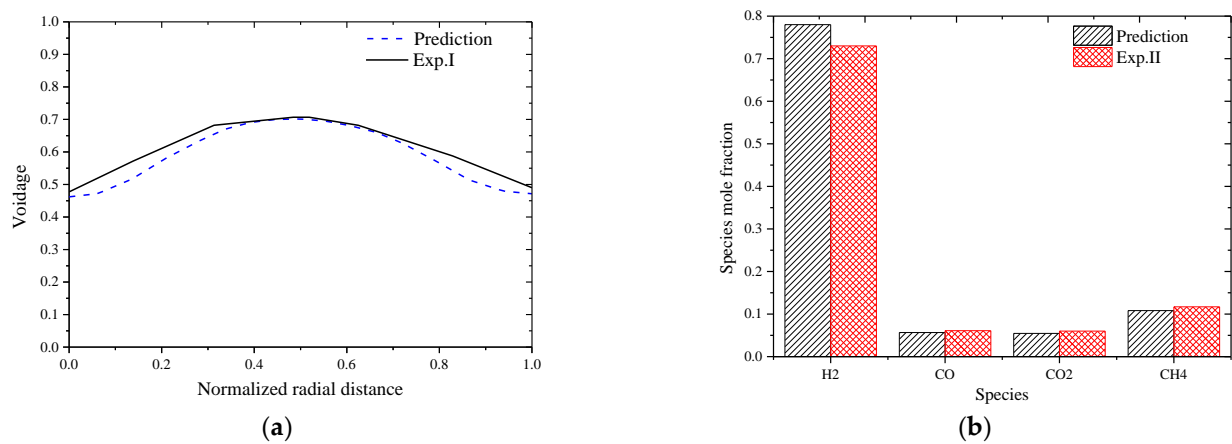


**Figure 2.** Comparison between predictions and experimental data. (a) Voidage comparison between prediction and Exp. I; (b) Species molar fraction comparison between prediction and Exp. II.

**Table 5.** Analysis of biomass.

	Proximate Analysis					Ultimate Analysis				
	$M_{ad}$	$FC_{ad}$	$V_{ad}$	$A_{ad}$	LHV (kJ/kg)	$C_d$	$H_d$	$O_d$	$N_d$	$S_d$
SC	5.87	55.04	31.90	7.18	28,844.7	76.36	4.52	10.41	0.98	0.10

### 3.2. Predictive Investigation of the QFBG

The initial and boundary operating parameters of the QFBG are listed in Table 6. The biomass feed rate is 4.5 kg/h, and its composition is given in Table 5. Under this condition, the operation characteristics of the QFBG are predicted and the key results are depicted in Figure 3a–h.

**Table 6.** The initial and boundary operating parameters of the QFBG.

Reactors	Bed Material	Bed Weight	Operation Temperature	Superficial Velocity	Inlet Gas
BFBG	CaO	17.7 kg	700 °C	0.4 m/s	H <sub>2</sub> O
BFBO	Mn <sub>3</sub> O <sub>4</sub>	28.1 kg	800 °C	0.5 m/s	Air

From panels (a–d) of Figure 3, it is seen that the main gas species have reached the gasifier outlet. From the mass fractions of H<sub>2</sub>, CH<sub>4</sub>, CO, and CO<sub>2</sub>, it can be deduced that the mole fractions of these species in dry gas are around 71.6%, 8.3%, 3.9%, and 16.2%, respectively. It is noted that the CO<sub>2</sub> mole fraction in the produced syngas is still a bit high, this is mainly because the system operates at atmospheric pressure. When the total pressure is 1 atm, the CO<sub>2</sub> partial pressure can be quite low because there can be a large amount of steam in the gasifier, leading to the CO<sub>2</sub> can only be partially absorbed by CaO. To solve this issue, it is suggested that the system operates at higher pressures. From panel (e) of Figure 3, it is seen that O<sub>2</sub> is generated and transported to the FFBC. This is caused by the reduction of Mn<sub>2</sub>O<sub>3</sub> in the FFBR. However, the O<sub>2</sub> concentration is still not high and can be increased by increasing the manganese ore circulating flux. From panel (f) of Figure 3, it is seen that the bed materials circulate well in the QFBG, indicating that the system can work reliably. From panel (g) of Figure 3, it is seen that the temperatures in BFBO and

FFBR are higher because the chemical looping air separation process with manganese ore as bed material operates at around 1050 K, while the dual bed gasification process with limestone as bed material operates at around 923 K. From panel (h) of Figure 3, it is seen that the highest static pressure appears at the lowest point of QFBG and the pressure drop of chemical looping air separation section is higher. This is because the particles are all fluidized in the connected pipes, and the manganese bed material is heavier.

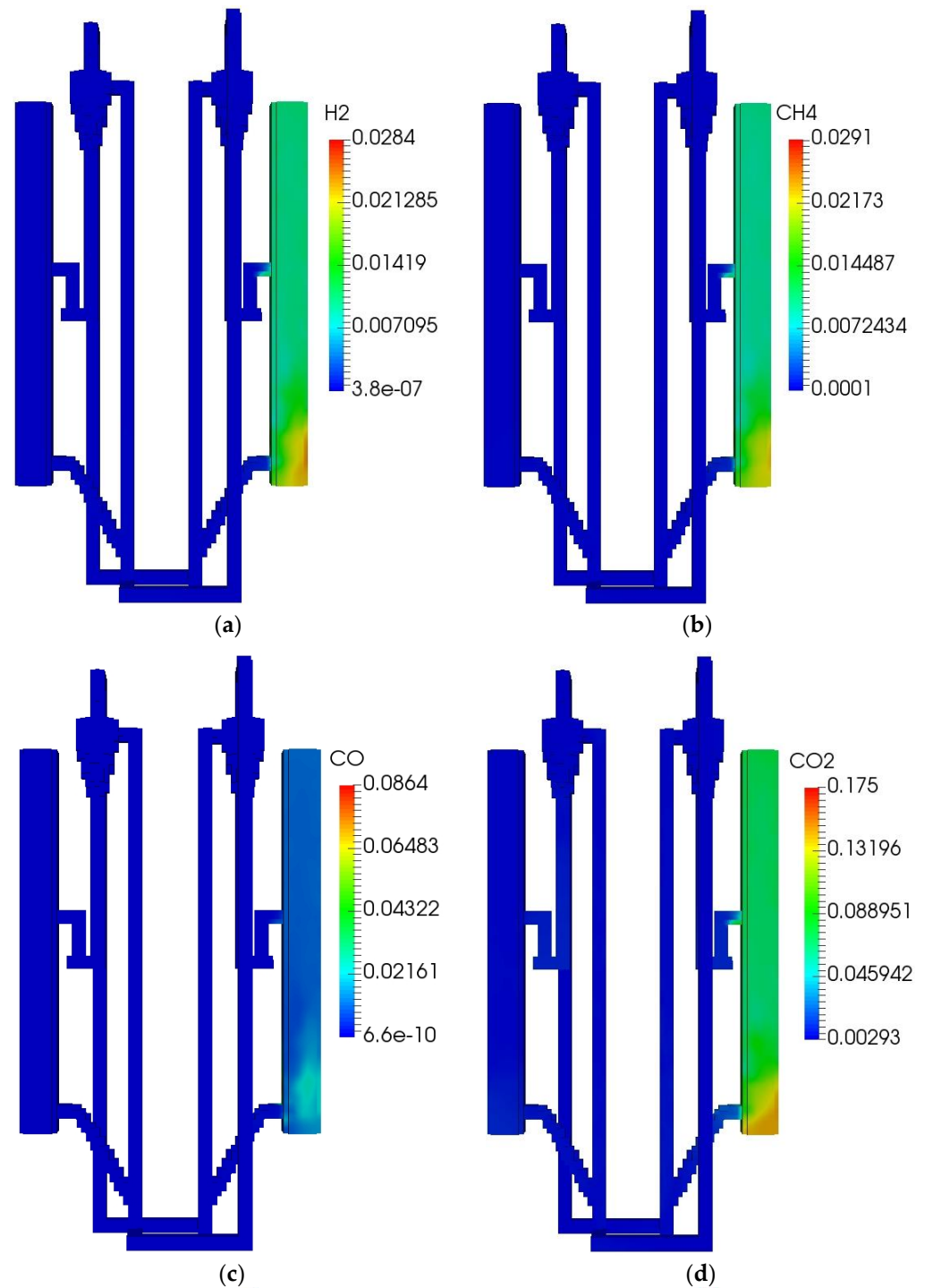
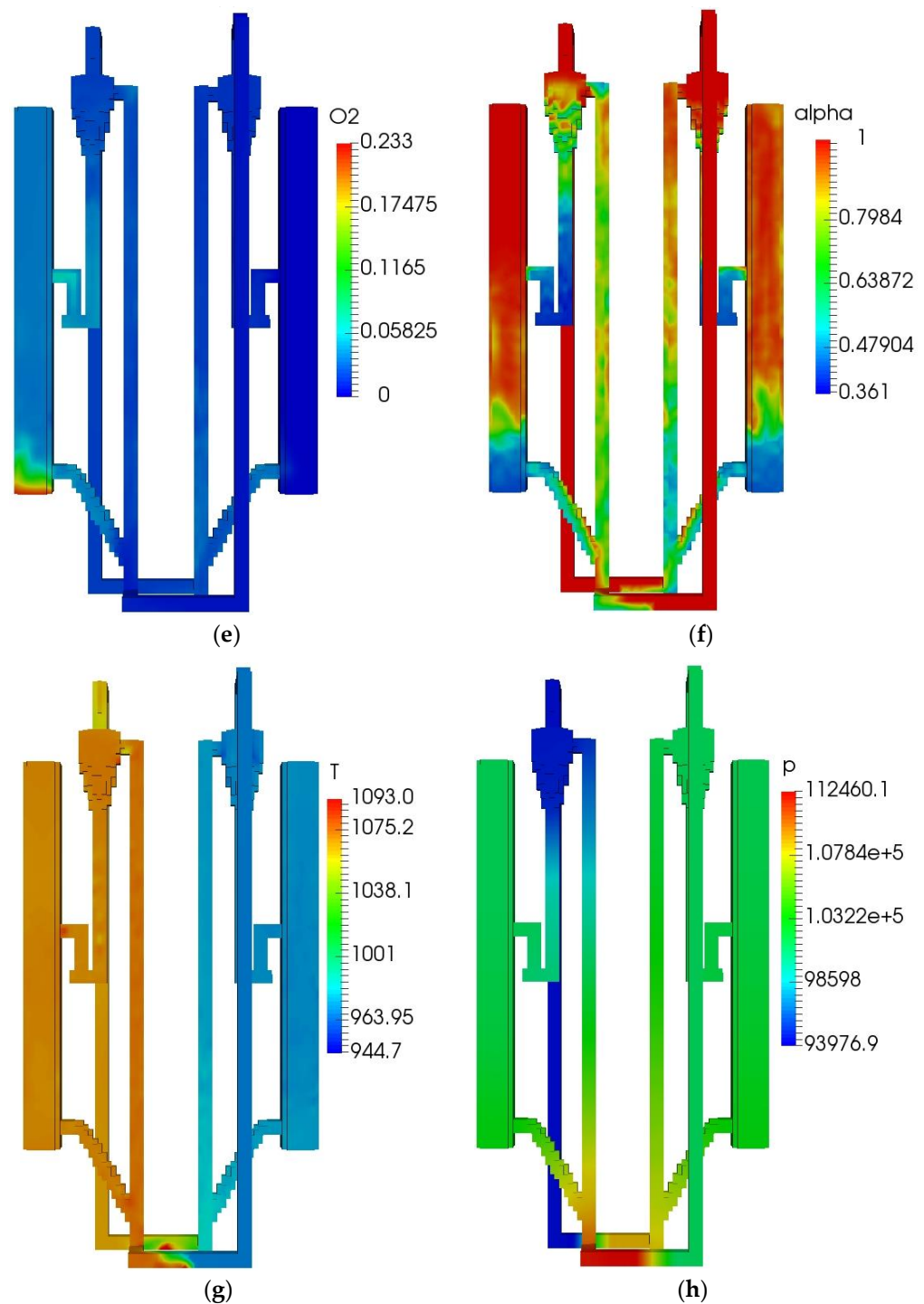


Figure 3. Cont.





**Figure 3.** QFBG operation results. (a) H<sub>2</sub> mass fraction; (b) CH<sub>4</sub> mass fraction; (c) CO mass fraction; (d) CO<sub>2</sub> mass fraction; (e) O<sub>2</sub> mass fraction; (f) Voidage distribution; (g) Temperature distribution; (h) Static pressure distribution.

#### 4. Conclusions

To study of operation characteristics of the quadruple fluidized bed gasifier (QFBG), a new solver based on the multiphase particle in cell scheme is built and accounts for the biomass pyrolysis, char gasification, gases species homogeneous reactions, CaO carbonation, CaCO<sub>3</sub> calcination, Mn<sub>2</sub>O<sub>3</sub> reduction, and Mn<sub>3</sub>O<sub>4</sub> oxidation. The solver is then validated against reported experimental data and finally used to predict the QFBG operation property. From this research, the key conclusions can be drawn as follows:

- (1) The new solver can give reliable predictions for the complex physicochemical processes in QFBG.
- (2) The QFBG works stably and the mole fractions of H<sub>2</sub>, CH<sub>4</sub>, CO, and CO<sub>2</sub> in dry gas are around 71.6%, 8.3%, 3.9%, and 16.2%, respectively, when the QFBG works at atmospheric pressure.
- (3) The QFBG performance can be further increased by increasing the operation pressure and the bed material circulating flux.

**Author Contributions:** Conceptualization, L.Y. and Z.J.; methodology, L.Y. and Z.J.; software, L.Y. and Z.J.; validation, L.Y. and Z.J.; formal analysis, L.Y. and Z.J.; investigation, Z.J.; resources, L.Y.; data curation, L.Y. and Z.J.; writing—original draft preparation, L.Y., Z.J., Z.W., B.H. and B.F.; writing—review and editing, L.Y. and B.F.; visualization, L.Y. and B.F.; supervision, L.Y.; project administration, L.Y.; funding acquisition, L.Y. All authors have read and agreed to the published version of the manuscript.

**Funding:** National Natural Science Foundation of China (NSFC, 51706012).

**Data Availability Statement:** Data will be available upon request from the corresponding authors.

**Acknowledgments:** The authors gratefully acknowledge financial support from the National Natural Science Foundation of China (NSFC, 51706012) for this work.

**Conflicts of Interest:** The authors declare no conflict of interest.

## Nomenclature

### Parameters

$A$	particle acceleration, $m/s^2$
$A_{ad}$	ash mass fraction in air-dried basis
$A_s$	particle surface area, $m^2$
$C_{CO_2}$	CO <sub>2</sub> concentration, $kmol/m^3$
$C_{CO_2,eq}$	CO <sub>2</sub> concentration at the equilibrium state, $kmol/m^3$
$C_d$	carbon mass fraction in dry basis
$C_{O_2}$	oxygen concentrations, $mol/m^3$
$C_{O_2,eq}$	oxygen concentration at the equilibrium state, $mol/m^3$
$d_p$	particle diameter, $m$
$D$	effective mass diffusivity, $m^2/s$
$D_{i,m}$	vapor diffusion coefficient, $m^2/s$
$D_s$	momentum transfer coefficient, $1/s$
$F$	momentum transfer rate, $N/m^3$
$FC_{ad}$	fixed carbon mass fraction in air-dried basis
$F_s$	particle friction per unit mass, $N/kg$
$g$	gravitational acceleration, $m/s^2$
$h_g$	gas enthalpy, $J/kg$
$H_d$	hydrogen mass fraction in dry basis
$k$	turbulence kinetic energy, $m^2/s^2$
$m_{CaO}$	mass flow rate of CaO, $kg/s$
$m_{devol}$	residual volatile mass, $kg$
$M_{ad}$	moisture mass fraction in air-dried basis
$M_w$	H <sub>2</sub> O molar weight, $kg/mol$
$N_d$	nitrogen mass fraction in dry basis
$O_d$	oxygen mass fraction in dry basis
$p$	gas pressure, $pa$
$P_{CO_2}$	CO <sub>2</sub> partial pressure, $atm$
$P_{CO_2,eq}$	CO <sub>2</sub> partial pressure at the equilibrium state, $atm$
$P_s$	particle stress coefficient, $pa$
$p^{sat}$	saturation pressure, $pa$
$\dot{q}_D$	enthalpy diffusion source, $W/m^3$

$\dot{Q}$	radiation source, $W/m^3$
$R$	universal gas constant, 8.3145 J/K
$S_d$	sulfur mass fraction in dry basis
$S_{gm}$	mass source, $kg/m^3/s$
$S_h$	homogeneous reaction enthalpy source, $W/m^3$
$Sh_{AB}$	Sherwood number
$S_{h,p}$	heterogeneous reaction enthalpy source, $W/m^3$
$T$	residence time, s
$T_g$	gas temperature, K
$T_p$	particle temperature, K
$T_\infty$	bulk temperature of gas, K
$u_g$	gas velocity, m/s
$u_s$	particle velocity, m/s
$\mu_t$	turbulent viscosity, $kg/m/s$
$V_{ad}$	volatile mass fraction in air-dried basis
$x_{cal}$	conversion of $CaCO_3$
$X_i$	bulk mole fraction of species i
$x_{Mn_2}$	conversion of $Mn_2O_3$
$Y_{g,i}$	mass fraction of species i
<i>Greek symbols</i>	
$\beta$	coefficient to calculate particle stress
$\gamma$	coefficient to calculate particle stress
$\delta$	Kronecker delta
$\delta\dot{m}_{i,chem}$	production rate of species i due to homogeneous reactions, $kg/m^3/s$
$\delta\dot{m}_{p,i,chem}$	production rate of species i due to heterogeneous reactions, $kg/m^3/s$
$\varepsilon$	turbulence dissipation rate, $m^2/s^3$
$\theta_{cp}$	packed particle volume fraction
$\theta_g$	gas volume fraction
$\theta_s$	solids volume fraction
$\lambda_g$	thermal conductivity, $W/m/K$
$\rho_g$	gas density, $kg/m^3$
$\rho_s$	solid density, $kg/m^3$
$\tau_D$	collision damping time, s
$\tau_g$	gas stress tensor, pa
$\tau_s$	particle normal stress, pa
$\phi$	viscous dissipation, $W/m^3$
<i>Abbreviations</i>	
BFBG	bubbling fluidized bed gasifier
BFBO	bubbling fluidized bed oxidation
CFD	computational fluid dynamics
DFBG	dual fluidized bed gasifier
FFBC	fast fluidized bed combustor
FFBR	fast fluidized bed reduction
GKT	granular kinetic theory
LHV	lower heating value
MPPIC	multi-phase particle in cell
QFBG	quadruple fluidized bed gasifier

## References

1. ElMekawy, A.; Hegab, H.M.; Mohanakrishna, G.; Elbaz, A.F.; Bulut, M.; Deepak, P. Technological advances in  $CO_2$  conversion electro-biorefinery: A step toward commercialization. *Bioresour. Technol.* **2016**, *215*, 357–370. [[CrossRef](#)] [[PubMed](#)]
2. Outcomes of the, U.N. Climate Change Conference in Paris. In Proceedings of the 21st Session of the Conference of the Parties to the United Nations Framework Convention on Climate Change (COP 21), Paris, France, 30 November–12 December 2015.
3. Marcucci, A.; Panos, E.; Kypreos, S.; Fragkos, P. Probabilistic assessment of realizing the 1.5 °C climate target. *Appl. Energy* **2019**, *239*, 239–251. [[CrossRef](#)]
4. Tian, X.; Wang, Y.; Zeng, Z.; Dai, L.; Peng, Y.; Jiang, L.; Yang, X.; Yue, L.; Liu, Y.; Ruan, R. Study on the mechanism of co-catalyzed pyrolysis of biomass by potassium and calcium. *Bioresour. Technol.* **2021**, *320*, 124415. [[CrossRef](#)] [[PubMed](#)]

5. Yan, L.B.; Cao, Y.; Li, X.Z.; He, B.S. Characterization of a dual fluidized bed gasifier with blended biomass/coal. *Bioresour. Technol.* **2018**, *254*, 97–106. [[CrossRef](#)] [[PubMed](#)]
6. Gunarathne, D.S.; Mellin, P.; Yang, W.; Pettersson, M.; Ljunggren, R. Performance of an effectively integrated biomass multi-stage gasification system and a steel industry heat treatment furnace. *Appl. Energy* **2016**, *170*, 353–361. [[CrossRef](#)]
7. Liu, H.; Saffaripour, M.; Mellin, P.; Grip, C.E.; Yang, W.; Blasiak, W. A thermodynamic study of hot syngas impurities in steel reheating furnaces—Corrosion and interaction with oxide scales. *Energy* **2014**, *77*, 352–361. [[CrossRef](#)]
8. Yan, L.; Lim, C.J.; Yue, G.; He, B.; Grace, J.R. One-dimensional modeling of a dual fluidized bed for biomass steam gasification. *Energy Convers. Manag.* **2016**, *127*, 612–622. [[CrossRef](#)]
9. Yan, L.; He, B. On a clean power generation system with the co-gasification of biomass and coal in a quadruple fluidized bed gasifier. *Bioresour. Technol.* **2017**, *235*, 113–121. [[CrossRef](#)] [[PubMed](#)]
10. Liu, G.; Zhao, Y.; Heberlein, S.; Veksha, A.; Giannis, A.; Chan, W.P.; Lim, T.T.; Lisak, G. Hydrogen and power co-production from autothermal biomass sorption enhanced chemical looping gasification: Thermodynamic modeling and comparative study. *Energy Convers. Manag.* **2022**, *269*, 16087. [[CrossRef](#)]
11. Pröll, T.; Hofbauer, H. H<sub>2</sub> rich syngas by selective CO<sub>2</sub> removal from biomass gasification in a dual fluidized bed system—Process modelling approach. *Fuel Process. Technol.* **2008**, *89*, 1207–1217. [[CrossRef](#)]
12. Koppatz, S.; Pfeifer, C.; Rauch, R.; Hofbauer, H.; Marquard-Moellenstedt, T.; Specht, M. H<sub>2</sub> rich product gas by steam gasification of biomass with in situ CO<sub>2</sub> absorption in a dual fluidized bed system of 8 MW fuel input. *Fuel Process. Technol.* **2009**, *90*, 914–921. [[CrossRef](#)]
13. Hejazi, B.; Grace, J.R.; Bi, X.; Mahecha-Botero, A. Steam gasification of biomass coupled with lime-based CO<sub>2</sub> capture in a dual fluidized bed reactor: A modeling study. *Fuel* **2014**, *117*, 1256–1266. [[CrossRef](#)]
14. Cormos, C. Energy and cost efficient manganese chemical looping air separation cycle for decarbonized power generation based on oxy-fuel combustion and gasification. *Energy* **2020**, *191*, 116579. [[CrossRef](#)]
15. Mei, D.; Soleimanisalim, A.H.; Linderholm, C.; Lyngfelt, A.; Mattisson, T. Reactivity and lifetime assessment of an oxygen releasable manganese ore with biomass fuels in a 10 kWth pilot rig for chemical looping combustion. *Fuel Process. Technol.* **2021**, *215*, 106743. [[CrossRef](#)]
16. Yan, L.B.; Cao, Y.; Li, X.Z.; He, B.S. On a carbon-negative energy production scheme via a quadruple fluidized bed gasifier. *Energy Convers. Manag.* **2018**, *171*, 326–338. [[CrossRef](#)]
17. Yan, L.B.; Cao, Y.; He, B.S. On the kinetic modeling of biomass/coal char co-gasification with steam. *Chem. Eng. J.* **2018**, *331*, 435–442. [[CrossRef](#)]
18. Yan, L.; Lim, C.J.; Yue, G.; He, B.; Grace, J.R. Simulation of biomass-steam gasification in fluidized bed reactors: Model setup, comparisons and preliminary predictions. *Bioresour. Technol.* **2016**, *221*, 625–635. [[CrossRef](#)] [[PubMed](#)]
19. Pissot, S.; Vilches, T.B.; Thunman, V.H.; Seemann, M. Dual Fluidized Bed Gasification Configurations for Carbon Recovery from Biomass. *Energy Fuel* **2020**, *34*, 16187–16200. [[CrossRef](#)]
20. Wang, S.; Yan, L.; Zhao, F.; Lu, H.; Sun, L.; Zhang, Q. Numerical simulation of hydrogen production via chemical looping-reforming in interconnected fluidized bed reactor. *Ind. Eng. Chem. Res.* **2014**, *53*, 4182–4191. [[CrossRef](#)]
21. Robertson, E.; Choudhury, V.; Bhushan, S.; Walters, D.K. Validation of OpenFOAM numerical methods and turbulence models for incompressible bluff body flows. *Comput. Fluids* **2015**, *123*, 122–145. [[CrossRef](#)]
22. Wen, C.Y.; Chaung, T.Z. Entrainment coal gasification modeling. *Ind. Eng. Chem. Proc. Des. Dev.* **1979**, *18*, 684–695. [[CrossRef](#)]
23. Ku, X.K.; Li, T.; Løvås, T. CFD-DEM simulation of biomass gasification with steam in a fluidized bed reactor. *Chem. Eng. Sci.* **2015**, *122*, 270–283. [[CrossRef](#)]
24. Gómez-Barea, A.; Leckner, B. Modeling of biomass gasification in fluidized bed. *Prog. Energy Combust. Sci.* **2010**, *36*, 444–509. [[CrossRef](#)]
25. Lanoye, L.; Vierendeels, J.; Segers, P.; Verdonck, P. Vascular fluid-structure-interaction using Fluent and Abaqus software. *J. Biomech.* **2006**, *39*, S440. [[CrossRef](#)]
26. OpenFOAM. *The Open Source CFD Toolbox, Ver. 3.0.0*; ESI Group: Paris, France, 2015.
27. Dubrawski, K.; Tebianian, S.; Bi, H.T.; Chaouki, J.; Ellis, N.; Gerspacher, R.; Jafari, R.; Kantzas, A.; Lim, C.; Patience, G.S.; et al. Traveling column for comparison of invasive and non-invasive fluidization voidage measurement techniques. *Powder Technol.* **2013**, *235*, 203–220. [[CrossRef](#)]
28. Pfeifer, C.; Puchner, B.; Hofbauer, H. Comparison of dual fluidized bed steam gasification of biomass with and without selective transport of CO<sub>2</sub>. *Chem. Eng. Sci.* **2009**, *64*, 5073–5083. [[CrossRef](#)]